The Journal of Experimental Biology 213, 2142-2153

doi:10.1242/jeb.029777

Kinematics of flight and the relationship to the vortex wake of a Pallas' long tongued bat (*Glossophaga soricina*)

Marta Wolf[1], L. Christoffer Johansson[1], Rhea von Busse[2], York Winter[2] and Anders Hedenström[1,*]

[1]Department of Biology, Lund University, Sölvegatan 37, SE-223 62 Lund, Sweden and [2]Department of Biology, Bielefeld University, D-33501 Bielefeld, Germany

*Author for correspondence (anders.hedenstrom@teorekol.lu.se)

Accepted 21 February 2010

SUMMARY

To obtain a full understanding of the aerodynamics of animal flight, the movement of the wings, the kinematics, needs to be connected to the wake left behind the animal. Here the detailed 3D wingbeat kinematics of bats, *Glossophaga soricina*, flying in a wind tunnel over a range of flight speeds (1–7 m s^{-1}) was determined from high-speed video. The results were compared with the wake geometry and quantitative wake measurements obtained simultaneously to the kinematics. The wingbeat kinematics varied gradually with flight speed and reflected the changes observed in the wake of the bats. In particular, several of the kinematic parameters reflected the differences in the function of the upstroke at low and high flight speeds. At lower flight speeds the bats use a pitch-up rotation to produce a backward flick which creates thrust and some weight support. At higher speeds this mechanism disappears and the upstroke generates weight support but no thrust. This is reflected by the changes in e.g. angle of attack, span ratio, camber and downstroke ratio. We also determined how different parameters vary throughout a wingbeat over the flight speeds studied. Both the camber and the angle of attack varied over the wingbeat differently at different speeds, suggesting active control of these parameters to adjust to the changing aerodynamic conditions. This study of the kinematics strongly indicates that the flight of bats is governed by an unsteady high-lift mechanism at low flight speeds and points to differences between birds and bats.

Supplementary material available online at http://jeb.biologists.org/cgi/content/full/213/12/2142/DC1

Key words: aerodynamics, bats, flight, kinematics, wake, wind tunnel.

INTRODUCTION

A flying animal has to produce support for its weight and thrust to overcome drag to move forward. Both of these forces are produced mainly by the lift generated by the flapping wings. The movement of the wings involves continuous changes of wing shape, area, velocity, angle of attack, etc. (Norberg, 1976a; Norberg, 1976b; Park et al., 2001; Rosén et al., 2004). Kinematic data offer an insight into the aerodynamic mechanisms of a flight pattern and are a natural first step when studying different flight styles. Such data can be collected without intrusive procedures, which is the reason why kinematics has a long history of detailed measurements. Previous studies have been performed on several bird species (e.g. Brown, 1953; Hedrick et al., 2002; Tobalske and Dial, 1996; Tobalske et al., 2007; Rosén et al., 2004; Rosén et al., 2007) as well as on a number of bat species (e.g. Aldridge, 1986; Aldridge, 1987; Hughes and Rayner, 1991; Hughes and Rayner, 1993; Norberg, 1972; Norberg, 1976a; Norberg, 1976b; Norberg et al., 1993; Lindhe-Norberg and Winter, 2006; Swartz et al., 2006).

Although the flight kinematics of the species used here, *Glossophaga soricina*, has been studied before (Norberg et al., 1993; Lindhe-Norberg and Winter, 2006), previous studies were performed in flight corridors and rooms where bats fly at freely chosen speeds. Here we present detailed kinematics over a range of flight speeds performed in a wind tunnel. The wind tunnel allows us to manipulate the flight speed and thus to monitor the change in kinematics more systematically over the whole range of studied flight speeds. As the bats are repeatedly obligated to fly at a certain flight speed we can choose consistently steady flight sequences for analysis, reducing the problems with accelerating and decelerating flight and allowing us to determine the variation in kinematics.

The limitation of kinematic studies is that the kinematic measurements alone are not sufficient to predict force generation and wake properties, which has been pointed out in a previous study of kinematics of bat flight (Lindhe-Norberg and Winter, 2006). Studies of the wake structure are therefore necessary; however, observations of the wake alone do not reveal much information about the kinematics of actuators. The best approach is therefore a combined study where wingbeat kinematics can be directly linked to the wake (Hubel et al., 2009). Sample kinematics and the structure of the wake have been shown to correlate in studies of flapping flight of a thrush nightingale *Luscinia luscina*, house martin *Delichon urbica* (Rosén et al., 2004; Rosén et al., 2007) and swifts *Apus apus* (Henningsson et al., 2008). Our study of *G. soricina* has shown that the wake of these bats differs in some aspects from those of these birds and includes several features not previously observed in any of the studied bird or bat species, such as individual vortex rings generated by each wing (Hedenström et al., 2007; Johansson et al., 2008). The wake properties have been described in detail in previous studies and here we present the detailed kinematics and relate it to some of the wake properties.

MATERIALS AND METHODS

Animals and morphology

Two adult Pallas' long-tongued bats *G. soricina* were used during this study, a female (bat 2) and a male (bat 1). The animals were born in captivity and kept in a bat-room at the Lund University

Wind Tunnel facility where they could fly freely (humidity approximately 50%, 24–27°C). The bats were time-shifted 12 h so that their active period was during the day and had free access to food (honey-water, Nectar Plus, Nekton, Pforzheim, Germany; baby formula and pollen) *ad libitum*, when not participating in the experiments. The experiments were approved by the Lund University ethical board (M153-05).

The bats were trained to fly at a feeder mounted in the test-section of the wind tunnel (a metal tube, 2 mm in diameter) connected to silicon tubes through which honey-water was provided during experiments (supplementary material Fig. S1). The temperature in the wind tunnel was kept at approximately 25°C. The bats approached the feeder by flying in the direction of the wind, passing the feeder and making a U-turn at the end of the test-section to approach the feeder from the downstream direction. The manner of the approach was different for the two bats. Bat 2 usually approached from below the feeder whereas bat 1 came in from above or at the same level as the feeder. The bats flew steadily for a period of 2–20 s while feeding and were individually recognized from the video recording. Between feeding bouts the bats roosted on a net 6 m upstream of the test-section.

We measured the morphometrics of the wing planform from in-flight images using Image J (http://rsb.info.nih.gov/ij/) following Pennycuick (Pennycuick, 1989). The bats were weighed before and after each experimental run. See Table 1 for morphological measurements of the bats.

Wind tunnel and methods

The technical details of the design and the performance of the wind tunnel have been described elsewhere (Pennycuick et al., 1997).

Kinematic data were collected using two synchronized high-speed cameras (Redlake MotionScope PCI 500, 250 Hz, 1/1250 s; Tallahassee, FL, USA) recording the bats from the dorsal [x–y] and side [x–z] views (supplementary material Fig. S1). Infrared lighting was used during filming (VDI-IR60F, Video Security Inc., Kaohsiung, Taiwan) to avoid disturbing the bats and to minimize interference with the DPIV (digital particle image velocimetry) measurements. Infrared filters [Schneider Optics, B&W, BW09249 092 (89B) Van Nuys, CA, USA] were used for the high-speed cameras to eliminate stray light from the laser used for DPIV data collection. Data for wake experiments were recorded simultaneously with kinematics, using DPIV. The methods and main results of the wake analysis have been presented elsewhere (Hedenström et al., 2007; Johansson et al., 2008).

Kinematics

The bats were studied at speeds from 1 to 7 m s^{-1}, with 0.5 m s^{-1} intervals. Although *G. soricina* has previously been shown to fly at speeds of up to 10.5 m s^{-1} (Winter, 1999), 7 m s^{-1} was the highest speed they would fly at in the wind tunnel possibly due to constraints in performing the U-turn before approaching the feeder. At every flight speed 10 stable sequences were chosen for further analysis. We could not obtain any sequences for bat 1 at 1.5 and 2 m s^{-1} and for bat 2 at 1.5 and 7 m s^{-1}. In the chosen sequence two stable wingbeats were selected for analysis, where the bat remained at its position in front of the feeder without drifting in any direction. The sequences were analysed starting at the beginning of a downstroke (the point of maximum elevation of the wingtip) and ending at the end of the second upstroke.

For each bat nine morphological points were tracked (Fig. 1 and supplementary material Table S1), digitized manually and transformed into three-dimensional coordinates by direct linear transformation (DLT) (Christoph Reinschmidt Matlab® routines; http://isbweb.org/software/movanal.html). For the digitized points the root mean square (r.m.s.) error was estimated using the least squares fit of the DLT calculation, representing digitization error as well as imperfection in the calibration. The error ranged between 0.8 mm at the shoulder (point 2) to 2.6 mm at the wingtip (point 5) (supplementary material Table S3). The 3D coordinates were used to estimate a number of kinematic parameters, including wingbeat frequency f (Hz) and wingbeat period T=1/f. The wingbeat frequency

Table 1. Morphometrics of bats

		Mean value		
	Symbol	Bat 1	Bat 2	Units
Body mass	m	0.0107±0.00007	0.0109±0.00004	kg
Wing span	b	0.237	0.243	m
Mean chord	c	0.037	0.038	m
Wing area	S	0.00884	0.00936	m^2
Aspect ratio	AR	6,4	6,3	
Wing loading	Q	1.21	1.17	kg m^{-2}

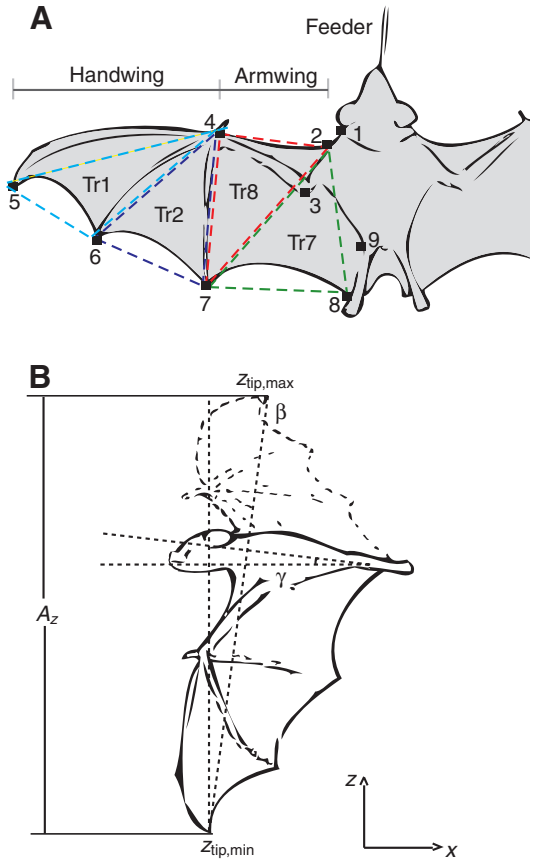

Fig. 1. Schematic drawing illustrating the definition of wingbeat kinematics parameters. (A) Morphological coordinates tracked on *Glossophaga soricina* bats for calculations of wingbeat kinematics, and triangles (Tr) used for angle of attack analysis. Definition of armwing and handwing used for span ratio calculations. (B) Tip-to-tip amplitude A_z, calculated from the wingtip positions at the maximum and minimum elevation, stroke plane angle β, calculated as the angle between the horizontal plane and a straight line through the maxima and minimum of z_{tip}, and the body tilt angle γ, defined as the angle between the horizontal and a straight line through the neck.

was derived from the power spectra of a Fourier transform of the vertical wingtip trace over time. The wingbeat period was divided into downstroke period T_d and upstroke period T_u, determined from the elevation of the wingtip, giving a downstroke ratio $\tau=T_d/T$.

The tip-to-tip amplitude A_z was calculated from the wingtip positions at the maximum and minimum elevation relative to the shoulder, during one wingbeat. The wing stroke amplitude θ was calculated using A_z, wing length and the horizontal amplitude A_x.

The stroke plane angle β was calculated as the angle between the horizontal plane and a straight line through the maximum and minimum vertical position of the wingtip relative to the shoulder, z_{tip}. The body tilt angle γ is the angle between the horizontal and a line connecting the neck and the leg in the [x–y] field (Fig. 1).

The span ratio SR is the ratio between the wingspan at mid-upstroke and mid-downstroke, calculated when the wing passes through the horizontal plane and levels with the shoulder. In order to measure which part of the wing is responsible for the changes of the wing form at different flight speeds, we also divided the wing into an armwing and a handwing. The armwing was defined as the part between the shoulder and the wrist and the handwing was defined as the part of the wing between the wingtip and the wrist (Fig. 1). We calculated a ratio separately for these parts (SR_{arm} and SR_{hand}) as the ratio between the wing length of the armwing and the handwing at mid-upstroke and mid-downstroke, respectively.

For the calculations of angle of attack α, the wing was divided into nine different triangles using the digitalized coordinates (supplementary material Table S2). For every triangle the centroid was defined and its velocity was calculated as the vector sum of forward and flapping speed. The angle of attack was calculated as the angle between the triangular plane and velocity vector for the centroid. The pattern of variation of angle of attack was similar for several of the triangles and therefore only four triangles were used for the final analysis, covering most of the wing surface (Fig. 1). The maximum and average angle of attack were calculated for the handwing (triangle 1, Fig. 1) for every downstroke.

Strouhal number

Strouhal number (St) is calculated using the flapping frequency (f), the tip-to-tip amplitude perpendicular to the forward motion (A_z) and the forward velocity (U) (Taylor et al., 2003):

$$St = fA_z / U . \quad (1)$$

Thus, fA_z represents half the mean vertical (for flight) velocity of the wing and U represents the horizontal velocity. In flying birds and bats, however, the stroke plane is not always vertical, causing the flapping to change the horizontal velocity of the wing as well as the vertical velocity. The effect is more pronounced at low flight speeds where the stroke plane is more tilted. This may result in an 'unfair' comparison with heaving plate studies. An alternative definition of St for the downstroke and upstroke is called for and can be defined as:

$$St_d = (A_z(1/\tau T)/2) / (U+(1/\tau T)A_x) = (A_z(f/\tau)/2) / (U+(f/\tau)A_x) , \quad (2)$$

$$St_u = A_z(f/1-\tau))/2) / (U-(f/(1-\tau))A_x) , \quad (3)$$

where τ is the downstroke ratio, T is the wingbeat period and A_x is the flapping amplitude in the horizontal direction. Once again St is half the mean vertical velocity of the wing divided by the mean horizontal velocity and therefore should be directly comparable with the standard St from heaving plate studies. This can also be seen by setting τ to 0.5 and A_x to 0, which would be the standard heaving plate setup. We have calculated both St and St_d for both bats to evaluate the different definitions of St.

Camber

We calculated a measure of camber for the armwing, for every wingbeat at all speeds using the coordinates 2, 3, 4, 7 and 9 (Fig. 1). Camber was defined as the elevation of the elbow over a plane created by the shoulder, the mean of the wrist and the shoulder and the mean of the fifth digit and the foot, divided by the distance between these last two points, representing the chord of the wing. This will tend to underestimate the camber because the skin membrane is 'concave' at the leading and trailing edge, making the true chord shorter than this estimate. However, this problem may not be as important here as the chord line is moved towards the elbow where the wing is generally less concave.

We calculated the mean and maximum camber for every wingbeat and the camber at mid-upstroke and mid-downstroke for both of the bats.

Wake comparison

For bat 2 we calculated the wingspan $2b$, at 4 and at 6.5 m s^{-1} and compared it with the width of the wake obtained from the transverse [y–z] view at the same speeds and for the same bat. The wake data were collected approximately 12 cm downstream of the wing trailing edge. The methods and analysis of the wake have been described in detail previously (Johansson et al., 2008).

The wake data were divided into six phases: beginning of downstroke (bd), mid-downstroke (md), end of downstroke (ed), beginning of upstroke (bu), mid-upstroke (mu) and end of upstroke (eu). The kinematic data for the wingspan were also divided into six phases per wingbeat, equal in duration, corresponding to the phases of the wake.

The normalized circulation measured in the wake can be used to estimate the lift coefficient (C_L) (Hoerner, 1975):

$$\Gamma/Uc = L/2qS = C_L/2 , \quad (4)$$

where Γ is the measured circulation, U is the flight speed, c is the mean chord, L is the lift and S is the wing area, and $q=(1/2)\rho U^2$ is the dynamic pressure. We used mean, normalized circulation values from the start vortex and the total measured circulation (Γ_{tot}) (Johansson et al., 2008) to estimate the lift coefficient and relate it to the kinematic measurements obtained in this study.

Statistics

All analyses were performed using linear mixed models using GLM procedure in JMP 8.0 (SAS Institute, Cary, NC, USA). Each of the flight variables was set as a dependent variable and the flight speed was set as covariate. The repeated measures setup with multiple wingbeats within sequences from the same bat was treated in the model by setting sequence, nested within individual as a random factor. This also allows us to determine any differences between the two bats. The low sample size results in some cases in low degrees of freedom which lowers the power of the test. However, this is properly treated in the model by setting sequence, nested within individual as a random factor, which allows us to compare the properties of regressions over speed and arrive at a significant result showing possible differences between the bats. The flight speed was initially included as a linear, quadratic and cubic term. Of the non-significant terms the least significant ones were then sequentially removed. All parameters showed a linear variation except for stroke plane angle, which varied with the square of speed. The values presented are means ± s.e.m.

Power functions were fitted using Microsoft Excel 2002, SP3.

RESULTS

Kinematics

A total of 110 sequences per bat were analysed, 10 for each of the 11 different flight speeds, with a total of 220 wingbeats for each of the bats. For the purpose of illustrating the wing movement, we chose characteristic sequences at low (1 m s^{-1}), medium (4 m s^{-1}) and high (6.5 m s^{-1}) speeds. For these we plotted the movement of the wrist, wingtip, fifth digit and foot, in relation to the shoulder, during two consecutive wingbeats, as seen from behind, side and top-view (Fig. 2 and supplementary material Fig. S2).

The wingbeat frequency decreased with increasing flight speed (R^2=0.93, P<0.001) (Fig. 3A). At the lowest flight speed (1 m s^{-1}) the frequency was 16.7 Hz for bat 1 and 17.6 Hz for bat 2. The frequency decreased to 13.4 Hz and 14.3 Hz, respectively at the highest common flight speed (6.5 m s^{-1}). There was a small difference in the wingbeat frequency between the two bats (P=0.01). The frequency of bat 1 varied as $17.1U^{-0.12}$ while the frequency for bat 2 varied as $17.8U^{-0.12}$.

During a downstroke the wings are extended and as the flight speed increased the extent of the vertical movement increased (Fig. 2A–C) and thus the wing stroke amplitude θ increased with increasing flight speed for both bats (R^2=0.56, P<0.0001) (Fig. 3B). There was no individual variation between the bats (P=0.06) and θ varied as $64.8U^{0.16}$.

At low speed the wings move further forward during a downstroke than at higher speeds (Fig. 2G–I). At the transition from the downstroke to the upstroke the wings go through a pitch-up rotation so that the handwing is flipped upside down (M.W., L.C.J., R.v.B., Y.W. and A.H., unpublished observation). During the upstroke the wings move upwards and backwards relative to the still air, which results in the wing moving in a clockwise loop as seen from the side (Fig. 2D–F).

As the flight speed increases the wingbeats become more vertical (Fig. 2D–F) and the wing is no longer flipped at the beginning of the upstroke. This transition occurs at flight speeds of approximately 3.0–3.5 m s^{-1} in *G. soricina*. Stroke plane angle thus increased with

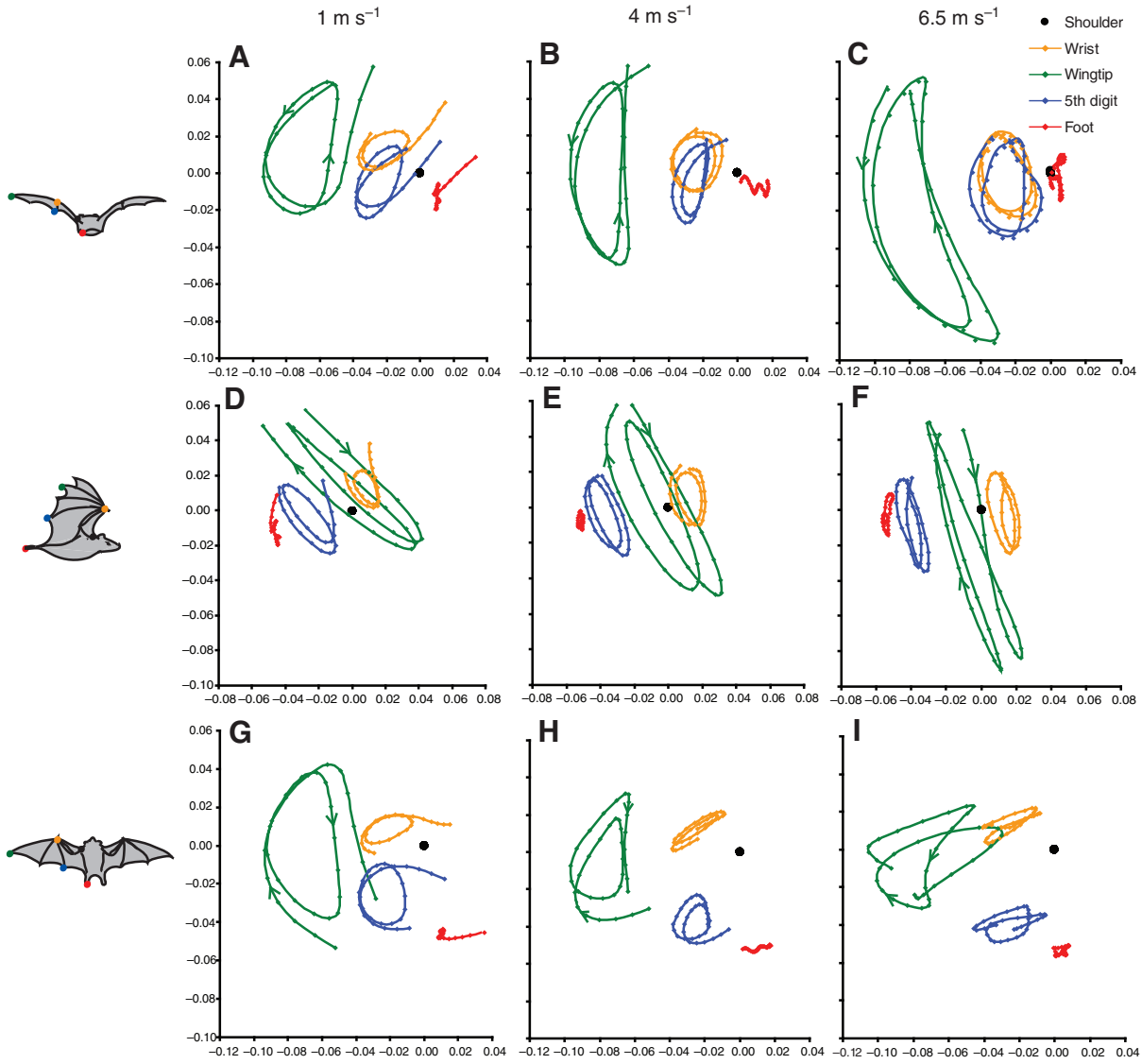

Fig. 2. Representative wing movement kinematics at low (1 m s^{-1}, 1st column), medium (4 m s^{-1}, 2nd column) and high flight speed (6.5 m s^{-1}, 3rd column) of *G. soricina*. The movement of the wrist, wingtip, fifth digit and foot, in relation to the shoulder (black circle), during two consecutive wingbeats, as seen from behind (A–C), side (D–F) and top-view (G–I). The axes are in metres where the shoulder represents the origin.

increasing flight speed but showed no difference between the two bats and varied with the square of flight speed (R^2=0.94, P<0.0001, $\beta=-0.35U^2+7.4U+44.1$) (Fig. 3C). The increase was more pronounced up to 5 m s^{-1} flight speed and more or less reached a plateau at higher flight speeds.

The body tilt angle varied with flight speed for bat 2 (R^2=0.46, P<0.001) but not for bat 1 (P=0.16), decreasing up to approximately 4.5 m s^{-1} and varying only slightly at higher flight speeds (Fig. 3D).

The downstroke ratio varied with flight speed in both bats (R^2=0.43, P<0.0001) (Fig. 3E). There was a small variation between the bats (P=0.02) and τ varied with $0.51U^{0.026}$ for bat 1 and $0.49U^{0.032}$ for bat 2. The downstroke ratio increased with increasing flight speed up to 3.5 m s^{-1} (bat 2) and 4.5 m s^{-1} (bat 1). At higher speeds there was a small tendency for decreasing τ in both bats (Fig. 3E and supplementary material Fig. S2).

The wingspan is reduced during an upstroke compared with the downstroke. At low flight speeds the wingspan is reduced more than at medium speeds (Fig. 2A–C). As the flight speed increases further the wingspan is reduced more at high speeds than at medium speeds, resulting in the largest upstroke wingspan at medium speeds (supplementary material Fig. S2). Thus the span ratio, SR, increased with increasing flight speed up to 3.5 m s^{-1} and showed a decreasing tendency at higher flight speeds (R^2=0.61, P<0.001) (Fig. 4A). There was no difference between the two bats (P=0.89).

The span ratio for the armwing, SR_{arm}, showed a similar pattern to SR (R^2=0.35, P<0.001), with span ratio increasing with increasing flight speed up to 4 m s^{-1} (bat 2) and 4.5 m s^{-1} (bat 1). There was no significant difference between the bats (P=0.18). At higher flight speeds SR_{arm} decreased slightly (Fig. 4B). Span ratio for the handwing, SR_{hand}, did not vary with flight speed (R^2=0.56, P=0.49) (Fig. 4C).

The angle of the attack varied throughout the wingbeat. Both the average and the maximum angle of attack of the downstroke decreased with increasing flight speed (AoA_{mean}: R^2=0.93, P<0.0001; AoA_{max}: R^2=0.93, P<0.0001) (Fig. 5). The maximum angle of attack was 50 and 59 deg for bat 1 and bat 2, respectively, at 1 m s^{-1}, and the average was 45 and 52 deg, respectively. At high flight speeds (6.5–7 m s^{-1}) the maximum angle of attack was 20 and 21 deg for bat 1 and bat 2, respectively. There was a difference in the average angle of attack between the bats (P<0.0001) as bat 2 was operating at a higher angle of attack, which was most pronounced at low flight speeds (Fig. 5A). The average angle of attack varied with flight speed as $58.5U^{-0.66}$ for bat 2 and $55.4U^{-0.65}$ for bat 1. There was no significant difference between the bats in the variation of the maximum angle of attack during a downstroke (P=0.044) but there was a similar trend that bat 2 operated at slightly lower angles of attack (Fig. 5B). The maximum angle of attack varied with the flight speed as $63.2U^{-0.55}$.

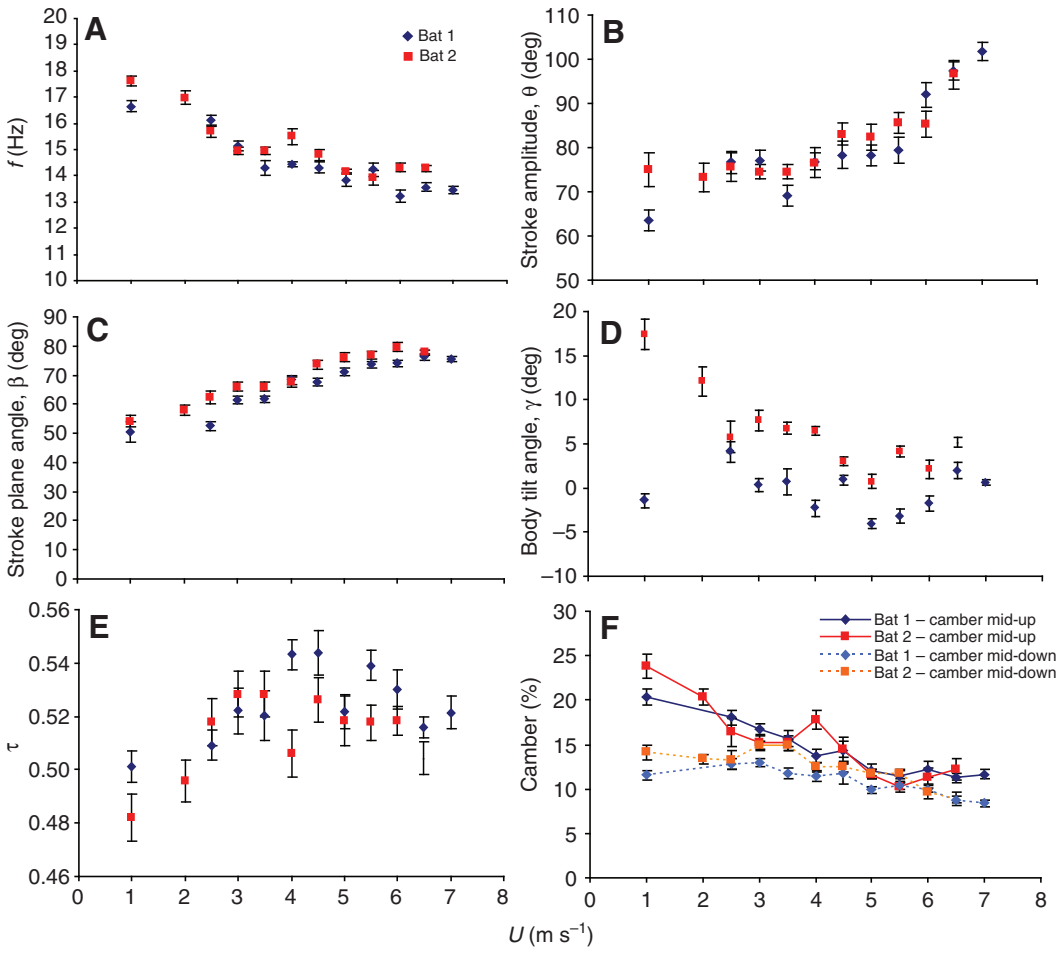

Fig. 3. Wingbeat frequency f (A), wing stroke amplitude θ (B), stroke plane angle β (C), body tilt angle γ (D), downstroke ratio τ (E) and camber at mid-upstroke and mid-downstroke (F) for both *G. soricina* bats, at flight speeds from 1 to 7 m s^{-1}. Values are means ± s.e.m. Key in A applies to A–E.

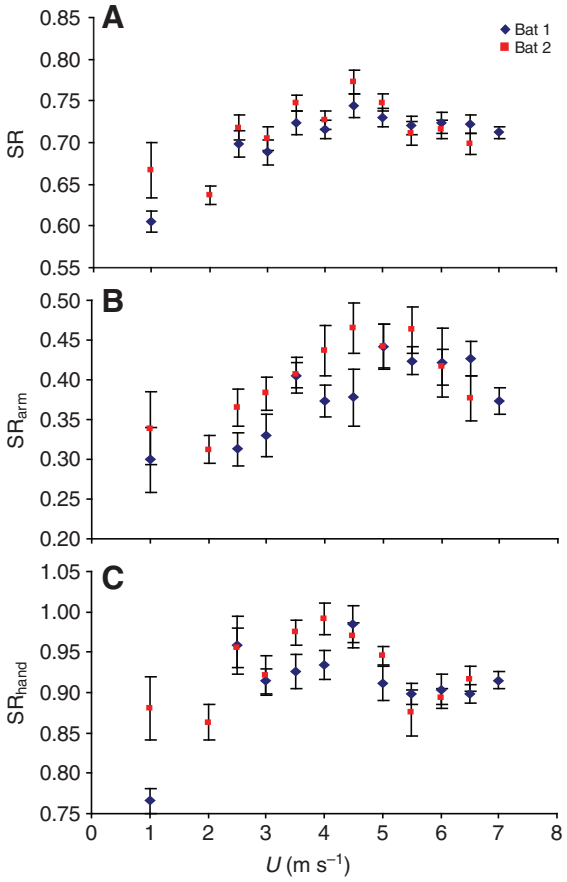

Fig. 4. Variation in span ratio SR (A), arm span ratio, i.e. wrist span (B) and hand span ratio, wingtip to wrist (C), for both bats, at flight speeds from 1 to 7 m s^{-1}. Values are means ± s.e.m.

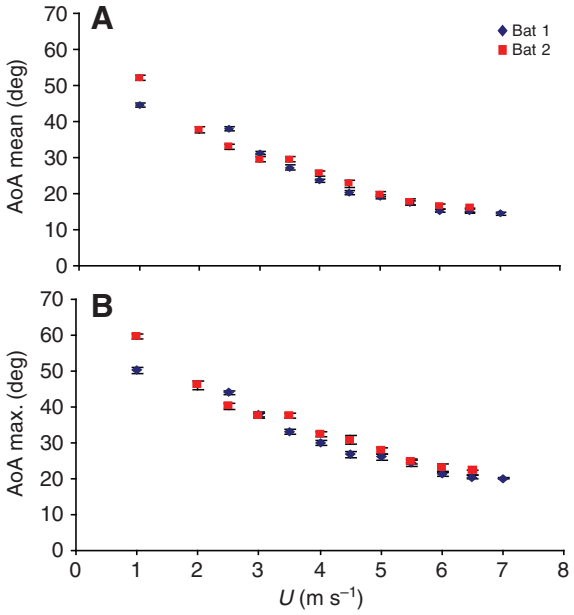

Fig. 5. Maximum and mean angle of attack (AoA, deg) during a downstroke for both *G. soricina* bats, at flight speeds from 1 to 7 m s^{-1}. Values are means ± s.e.m.

The changes of angle of attack during a wingbeat were quite dramatic at low flight speed (1 m s^{-1}). The angle of attack reached values of –10 to –70 deg for different parts of the wing during the upstroke while during the downstroke the angle of attack for most of the wing did not vary much and remained between 40 and 60 deg. This resulted in fast and 'strong' changes in the angle of attack at the transition between upstroke and downstroke and between downstroke and upstroke (Fig. 6).

The variation of the angle of attack for the triangles describing the handwing (triangle 1 and triangle 2, Fig. 1) was very similar, with the hand-most part displaying the largest values during the downstroke and the most negative values of angle of attack during the upstroke (Fig. 6). The armwing was described by two triangles, triangle 7 and triangle 8 (Fig. 1). The angle of attack for the innermost wing varied in a similar way to that of the handwing. The angle of attack for the part of the wing described by triangle 7 did not show the dramatic changes, although the variation was larger at low flight speeds. During the upstroke the angle of attack rarely reached negative values (Fig. 6).

At 4 m s^{-1}, changes of the angle of attack became less dramatic and the angle of attack varied between –20 and 40 deg for an entire wingbeat period. The angle of attack for the armwing and handwing varied in a similar pattern, with more negative angles of attack for the handwing during the upstroke (Fig. 6). The angle of attack of triangle 7 remained positive throughout the entire wingbeat, varying between 10 and 20 deg. The angle of attack of the handmost part of the wing, triangle 1, varied most among the wing segments, from 35 deg during downstroke to –20 deg during upstroke (Fig. 6).

At 6.5 m s^{-1} the variation of the angle of attack decreased even further to between –10 and 30 deg. Among the wing segments the hand part of the handwing varied most, between –10 and 30 deg. The angle of attack of the armwing (triangle 7) remained almost stable, fluctuating around 10 deg. The angle of attack of the innermost wing declined as well (Fig. 6).

Strouhal number

Strouhal number calculated in the traditional way (*St*) decreased with increasing flight speed (R^2=0.99, P=0.02) (Table 2). At speeds lower than 3.0–3.5 m s^{-1} the Strouhal number was higher than 0.4, and decreased at higher flight speeds with $1.26U^{-0.86}$; there was no statistical difference between the bats (P=0.76). Strouhal number for the downstroke (St_d) also decreased with increasing flight speed (R^2=0.83, P<0.0001); however, it remained between 0.2 and 0.4 at all flight speeds (Table 2). There was no significant difference between the two bats (P=0.24).

Camber

Camber varied with flight speed. Both the maximum and average camber during a wingbeat decreased as the flight speed increased (maximum camber, $Camber_{max}$: R^2=0.93, P=0.02; mean camber, $Camber_{mean}$: R^2=0.84, P<0.0001). The mean camber varied from 0.16 and 0.18, respectively, at the lowest speed, to 0.10 at the highest speed. The maximum camber ranged from 0.30 for bat 2 and 0.25 for bat 1, at low speed, to 0.15 at the highest speed. There was no significant difference between the bats (P=0.75).

The camber at mid-upstroke was about twice that at mid-downstroke at the lowest flight speed (Fig. 3F). As the flight speed increased the camber at mid-upstroke decreased from 0.20 and 0.24, respectively, to 0.12 (R^2=0.52, P<0.0001). The camber at mid-

Table 2. Strouhal number for the entire wingbeat and for the downstroke at different flight speeds

		1	2	2.5	3	3.5	4	4.5	5	5.5	6	6.5	7
Bat 1	*St*	**1.36**	–	**0.60**	**0.49**	0.37	0.36	0.33	0.28	0.28	0.26	0.27	0.25
	St_d	0.39	–	0.28	0.29	0.25	0.25	0.24	0.22	0.22	0.21	0.23	0.21
Bat 2	*St*	**1.36**	**0.67**	**0.61**	**0.55**	**0.45**	0.38	0.36	0.31	0.29	0.27	0.27	–
	St_d	0.30	0.33	0.33	0.32	0.29	0.27	0.26	0.24	0.24	0.22	0.23	–

St is the traditional Strouhal value for the entire wingbeat and St_d is the value for the downstroke Strouhal number. Bold numbers indicate when *St* lies outside the theoretical optima 0.2–0.4.
Fight speed is in m s^{-1}.

downstroke also decreased but the decline was much lower, ranging from 0.12 and 0.14 to 0.09 (R^2=0.64, P<0.0001). There was no significant difference between the bats for the camber at mid-downstroke (P=0.90). There was a difference in the variation of camber at mid-upstroke (P<0.0001), as bat 2 generally operated at higher mid-upstroke camber values at low and medium flight speeds (Fig. 3F).

Wake comparison

The variation of the width of the wake corresponded well to the change in the wingspan, at 4 and 6.5 m s^{-1} (Fig. 7). Both the wake width and the wingspan increased from the beginning of the downstroke to mid-downstroke and decreased towards the end of the downstroke. At the beginning of the upstroke both the wake width and the wingspan decreased further; however, the decrease in the wake width was larger than the decrease in the wingspan. Both the wake width and the wingspan increased at mid-upstroke compared with the beginning of upstroke. The increase of the wake width was, however, lower than the increase in the wingspan at 6.5 m s^{-1}. At the end of upstroke the wake width decreased, which was most pronounced at 4 m s^{-1}. The wingspan did not increase at the end of upstroke at 4 m s^{-1} but it did increase at 6.5 m s^{-1} (Fig. 7).

The statistical analysis of the normalized circulation and speed has been presented elsewhere (see Johansson et al., 2008). Both the normalized circulation of the start vortex (Γ/Uc) and the total measured circulation (Γ_{tot}/Uc) increased with increasing camber (R^2=0.56, P=0.0001; R^2=0.47, P=0.0008) and angle of attack (R^2=0.92, P<0.0001; R^2=0.80, P<0.0001). These two factors are correlated (Fig. 9C); however, statistically angle of attack had a larger effect on the circulation (Table 3).

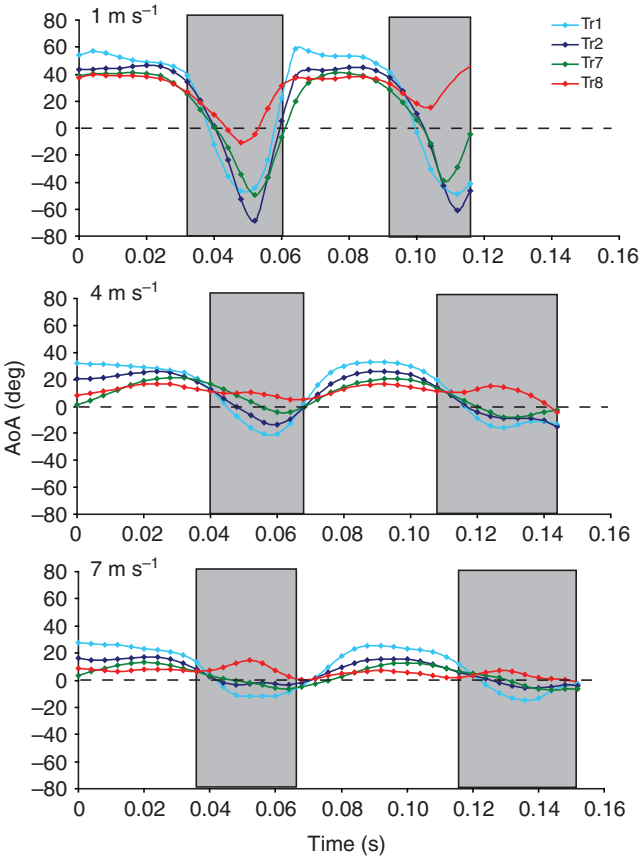

Fig. 6. Representative variation of angle of attack during two consecutive wingbeats for the four investigated triangles of a bat wing (Tr1, Tr2, Tr7 and Tr8) at low (1 m s^{-1}), medium (4 m s^{-1}) and high flight speed (6.5 m s^{-1}). Tr1 and Tr2 represent the handwing and Tr7 and Tr8 represent the armwing. The shaded areas indicate the upstroke.

DISCUSSION

The design of this study allowed for a thorough investigation of the flight kinematics of the individual bats over a range of flight speeds. The kinematics of *G. soricina* have been examined previously (von Helversen, 1986; Norberg, 1993; Lindhe-Norberg and Winter, 2006), although the previous studies examined a more restricted speed range compared with that in the present study. Our experimental setup allowed control of flight speed, enabling kinematics to be monitored repeatedly at fixed points in the entire range of flight speeds. The study is based on two individuals only and such low sample size suggests the results should be interpreted with some caution. However, the overall similarity of the patterns in terms of how the wingbeat kinematics varies over speed between the two individuals indicates that the results are consistent.

Kinematics

We found that the wingbeat frequency decreased with increasing flight speed ($f \propto U^{-0.12}$), which is consistent with previous findings in *G. soricina* (Lindhe-Norberg and Winter, 2006). This differs from the findings in birds where no change in wingbeat frequency with flight speed was found in the thrush nightingale (Rosén et al., 2004), the black-billed magpie *Pica pica*, the pigeon *Columba livia* (Tobalske and Dial, 1996), and the rufous hummingbird *Selasphorus rufus* (Tobalske et al., 2007).

Table 3. *P*-values for comparison between the normalized wake and camber and angle of attack

	Γ/Uc	Γ_{tot}/Uc
Intercept	0.0974	0.8185
Angle of attack (AoA)	**<0.0001** (0.92)	**0.0002** (0.80)
Camber	0.5832 (0.56)	0.5629 (0.47)
AoA × camber	0.7771	0.8455

P-values in bold are significant. R^2 values are given in parentheses.
Γ, circulation; *U*, speed; *c*, mean chord; subscript tot, total.

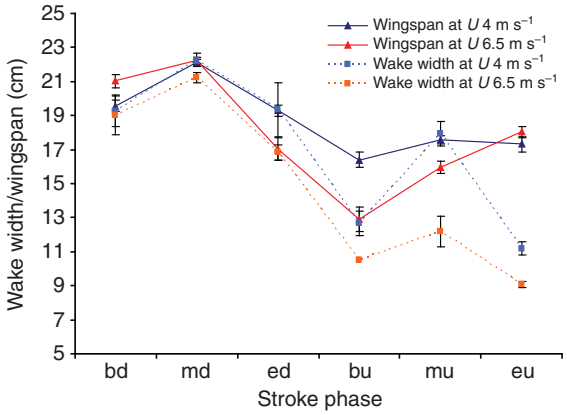

Fig. 7. Wingspan and wake width for bat 2 at 4 m s^{-1} and 6.5 m s^{-1} during six phases of a wing stroke: beginning of downstroke (bd), middle of downstroke (md), end of downstroke (ed), beginning of upstroke (bu), middle of upstroke (mu) and end of upstroke (eu). Values are means ± s.e.m.

According to the predictions made by Lindhe-Norberg and Winter (Lindhe-Norberg and Winter, 2006), *G. soricina* should fly at a theoretical minimum power speed U_{mp}≈6 m s^{-1}, with a wingbeat frequency of 9.5–10.3 Hz, depending on the body mass. To allow comparison of wingbeat frequency at a calculated U_{mp} with the results of Lindhe-Norberg and Winter (Lindhe-Norberg and Winter, 2006), we used Pennycuick's program [Flight 1.22 (Pennycuick, 1989)]. The program predicts that our bats should fly at 9.65 Hz at U_{mp}=6.40 (bat 2) and 10.8 Hz at U_{mp}=7.10 (bat 1). Both our bats were in the same range of body mass as the bats used by Lindhe-Norberg and Winter (Lindhe-Norberg and Winter, 2006), but were flying with a wingbeat frequency of 13.4–14.3 Hz at the high flight speeds (6.5–7.0 m s^{-1}). There was a small difference between the bats as the slightly heavier bat 2 was operating at a somewhat higher wingbeat frequency. Our bats operated at higher wingbeat frequencies at all flight speeds than those studied by Lindhe Norberg and Winter (Lindhe Norberg and Winter, 2006), which may be a wind tunnel effect created by the bats manoeuvring to maintain their position in front of the feeder.

There was a difference in the body tilt angle between the two bats at the lowest flight speed which might originate from a different flight style when approaching the feeder. Both bats were flying past the feeder and making a U-turn, but bat 2 always approached the feeder from underneath while bat 1 approached the feeder from above or at the same level as the feeder. The difference was most pronounced at the lowest speeds and as the flight speed increased the approach style of the two bats converged and the body posture of bat 2 became more horizontal.

Wing stroke amplitude increased with increasing flight speed, which is compatible with the results reported for other bats and birds (Park et al., 2001; Hedrick et al., 2002; Lindhe-Norberg and Winter, 2006; Bullen and McKenzie, 2002). The stroke plane angle also increased with increasing flight speed, which has previously been shown (Lindhe-Norberg and Winter, 2006). The standard explanation is that these changes in wingbeat kinematics are associated with the different requirements for lift and thrust production at different flight speeds (but see below for an alternative hypothesis). At low flight speeds the production of lift to create weight support is more difficult and a more horizontal wingbeat is expected. At higher speeds, when profile and parasite drag become increasingly important, the need to produce thrust is more critical and a more vertical wingbeat and higher amplitude is expected. In flying animals the wing stroke amplitude, body tilt angle and stroke plane angle vary to satisfy these different demands (Park et al., 2001; Tobalske and Dial, 1996; Rosén et al., 2007).

The downstroke ratio increased with increasing flight speed for both bats at low speeds; however, at higher flight speeds there is a clear tendency for the downstroke ratio to decrease with further increases in speed (Fig. 3E). The downstroke ratio has been shown to decrease with increasing flight speed in magpies and pigeons (Tobalske and Dial, 1996), barn swallows *Hirundo rustica* (Park et al., 2001), cockatiels *Nymphicus hollandicus* (Hedrick et al., 2002), robins *Erithacus rubecula* (Hedenström et al., 2006) and house martins (Rosén et al., 2007). A decreasing downstroke ratio indicates an increasing contribution to weight support by the upstroke and an increased production of thrust during the downstroke, and our bats follow the same pattern as the birds at high speed.

At low flight speeds, which have not been studied for most of these birds, the downstroke generates weight support and some thrust and during the upstroke some thrust and weight support is produced. Kinematic studies of rufous hummingbirds (Tobalske et al., 2007) show a similar increase in the downstroke ratio at the lower flight speeds. However, in hummingbirds the downstroke ratio continues to increase up to the highest flight speed studied (12 m s^{-1}), whereas in our bats the downstroke ratio appears to decrease at higher speeds. We have previously shown that these bats have an active upstroke at all flight speeds, but the mechanism of lift production differs between low and high speeds (Hedenström et al., 2007; Johansson et al., 2008). The backward flick mentioned earlier disappears at flight speeds around 3.0–3.5 m s^{-1}. At flight speeds up to approximately 3.5 m s^{-1} (bat 2) and 4.5 m s^{-1} (bat 1) the downstroke ratio increases as the fraction of the wingbeat occupied by the upstroke decreases when the wing pitch-up rotation disappears. The change in the downstroke ratio visibly reflects the pattern found in our previous studies of the wake of *G. soricina* (Hedenström et al., 2007; Johansson et al., 2008).

The span ratio increased with increasing flight speed from low to medium flight speeds and decreased at higher flight speeds (Fig. 4). Lindhe-Norberg and Winter found a correlation between span ratio and wingbeat frequency, but not between span ratio and flight speed, for *G. soricina* (Lindhe-Norberg and Winter, 2006). However, this result was based on just 17 flights over the speed range, which may not be enough to observe the variations in span ratio. Also, span ratio does not vary according to a power function, and fitting a power function to the data (as Lindhe-Norberg and Winter did) may result in a non-significant result. Span ratio has been reported to increase with increasing flight speed in a number of bird species (Tobalske and Dial, 1996; Hedrick et al., 2002; Rosén et al., 2004; Rosén et al., 2007). This change in the wingspan is usually associated with a reduction of the wingspan during the upstroke at low speeds, which is essential for the generation of net positive thrust and for overcoming drag. The span ratio of our bats varied between approximately 0.6 at the lowest speeds and 0.70–0.75 at medium and high speeds. This is higher than the span ratio reported for most bird species (Tobalske et al., 2007). For thrush nightingale flying at a speed of 5–10 m s^{-1} the span ratio varied from approximately 0.36 to 0.44 (Rosén et al., 2004) and SR=0.3–0.4 for house martin at 4–10 m s^{-1} (Rosén et al., 2007). A similar value (SR≈0.7) to that of our bats has been reported for swifts flying at 8.0–9.2 m s^{-1} (Henningsson et al., 2008). The swifts showed no variation in the span ratio over this narrow range of flight speeds, which is probably due to their unique wing morphology, with quite

rigid wings that are difficult to flex. Tobalske and colleagues (Tobalske et al., 2007) showed that rufous hummingbirds, which also have rigid wings, had little variation in the span ratio and exhibited the highest observed span ratio among bird species (SR≈0.2–0.4). The difference between the Pallas' long-tongued bats studied here and the bird species studied by others to date may similarly depend on differences in the wing morphology. The span ratio in birds is generated as the handwing is swept almost straight backwards and the arm is then flexed to various degrees to fine tune the span ratio (Hedrick et al., 2002). Bats have membranous wings that are flexed to a lesser degree and sweeping the handwing would mean collapsing the membrane, which would most likely result in a 'flag effect' increasing drag and decreasing lift production (Vogel, 1994). It is also likely that it would result in adverse effects for force generation when the wings are subsequently unfolded to start generating forces again.

We also examined the span ratio for the armwing (wrist span) and for the handwing separately to determine whether the handwing is flexed or not during the upstroke. The overall pattern of the variation in the span ratio is mainly explained by the changes of the armwing span during the upstroke, which increases with increasing flight speed of 3.5–5.0 m s^{-1}. The lower SR_{arm}, at low speeds, reflects the twisting motion of the wing to produce the back-flick of its hand-most part. At higher speeds the SR_{arm} shows a tendency to decrease as the wingspan is reduced during the upstroke (Fig. 4). The SR_{hand} was generally a lot higher than the SR_{arm} but was also lower at the low flight speeds, increasing to approximately 0.95 at 2.5 m s^{-1}. The lower values at the low speed are probably due to the motion of the wing when going through the pitch-up rotation during the upstroke. We thus conclude that in *G. soricina* a reduction in span ratio during the upstroke is mainly accomplished by reducing the span of the armwing, while keeping the handwing membrane relatively stretched.

Angle of attack

Both the average and maximum angle of attack during the downstroke decreased with increasing flight speed. At the lowest flight speed the variations in the angle of attack were quite high, ranging from almost –70 to 60 deg. These values are very high compared with those used by engineered aircraft airfoils, which usually operate at angles of attack between 0 and 15 deg (e.g. McCormick, 1995; Laitone, 1997). For steady-state airfoils, increasing the angle of attack will increase the lift of a given airfoil up to a critical angle of attack. At that point the flow starts to separate, the lift drops and the wing is said to have stalled. The very high values of angle of attack of bat wings would thus suggest a separated flow. Flow visualization directly above the wing surface of *G. soricina* bats has also shown that the flow separates at the leading edge, but instead of a loss of lift these bats are able to stabilize leading edge vortices during slow forward flight that contribute as much as 40% of the total lift (Muijres et al., 2008). Despite the high angles of attack and camber the airflow passing over the leading edge vortex reattaches smoothly to the wing behind the leading edge vortex and hence avoids separation at the trailing edge (Muijres et al., 2008).

We also found that the angle of attack varied substantially over the course of a wingbeat. The angle of attack was highest and stable during a downstroke and changed mostly during an upstroke, becoming increasingly more negative up to approximately mid-upstroke. Then it changed again and progressed towards higher values at the end of the upstroke, becoming positive at the beginning of the downstroke. Similar results have also been shown for the chocolate wattled bat (*Chalinolobus morio*) and smaller horseshoe bat (*Rhinolophus megaphyllus*) (Swartz et al., 2006) and some bird species, e.g. rufous hummingbirds (Tobalske et al., 2007), cockatiels and ringed turtle-doves *Streptopelia risoria* (Hedrick et al., 2002). For triangle 8 (Fig. 1) the angle of attack did not vary as much and remained positive for most of the time. This is partly due to the fact that this area includes the rigid parts of the wing such as the elbow and the thumb, and the membrane included actually consists of two different parts; a part of the wing membrane and the propatagium. Thus the variation of the angle of attack is limited by the rigidity of this part of the wing.

At the lowest speed the values of angle of attack were highly negative during the upstroke, reaching approximately –70 deg for the distal part of the wing. The extremely negative values are due to the back-flick motion of the wing causing the air to meet the wing's upper surface. As the speed is increased the negative angle of attack is decreased and was negative only for the handmost part of the wing. Variations of a similar magnitude and pattern have been shown for hovering hummingbirds (Tobalske et al., 2007). Muijres and colleagues also examined the variation in the angle of attack at mid-downstroke along the span of a slow flying (1 m s^{-1}) *G. soricina*, using a different method and found values corresponding well to our estimates (Muijres et al., 2008). They also found that the values of angle of attack were similar for the whole wing, which is supported here as the angle of attack of the different investigated triangles varied quite homogeneously at mid-downstroke at slow flight speed (1 m s^{-1}).

Strouhal number

Strouhal number is a dimensionless parameter frequently used as an index of the characteristics and steadiness of the flow. It has been suggested that there is a favourable region for flight, which falls in the interval $0.2<St<0.4$ (Taylor et al., 2003). Force production outside this region may be unfavourably influenced by the unsteadiness of the flow (see below) (Anderson et al., 1998; Wang, 2000; Nudds et al., 2004) and result in chaotic wakes and force generation (Lentik et al., 2010). For our bats *St* varied between 0.25 and 1.36, with a negative trend with increasing flight speed (Table 2), which was also found by Lindhe-Norberg and Winter (Lindhe-Norberg and Winter, 2006). At speeds lower than 3.5 m s^{-1} the bats were operating at *St* higher than the suggested favourable region, which would indicate suboptimal flow conditions. On the other hand using our alternative definition (St_d) results in the bats operating within a favourable *St* range during the downstroke at all flight speeds studied here (Table 2).

The relationship between *St* and the angle of attack on the vorticity shedding in the wake has previously been studied on heaving plates (Anderson et al., 1998) (see also Lentik et al., 2010). We compared our wake data from the bats with a figure of wake patterns as a function of the *St* and angle of attack (Fig. 8) (modified from Anderson et al., 1998). We have previously described a wake pattern for the bats at 2–2.5 m s^{-1} (*St* is 0.61–0.67, mean angle of attack 36–42 deg and maximum angle of attack 42–50 deg) that consists of 'double start vortices' (Johansson et al., 2008), which resembles the wake pattern shown in areas D and F of Fig. 8. Wakes in areas D and F are not favourable as they result in the formation and shedding of trailing edge vortices, which reduce the propulsive efficiency. We do not find this wake pattern at 3 m s^{-1} ($St\approx0.55$; $AoA_{mean}\approx32$ deg; $AoA_{max}\approx38$ deg), which would be expected from the combination of *St* and angle of attack (Fig. 8). However, Anderson and colleagues (Anderson et al., 1998) studied heaving, symmetrical profiles and the cambered wing profiles of bats might behave differently. It could also be that the bats, by changing the

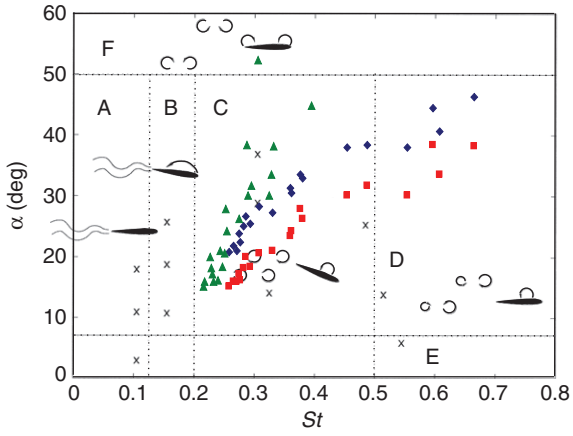

Fig. 8. Wake patterns as a function of Strouhal number *St* and angle of attack α, modified from Anderson (Anderson, 1998). Capital letters represent regions where the different wake patterns, illustrated by the arrows and airfoils, have been observed. The black crosses mark the location of experiments reported in the original paper. Our data are fitted into the figure; red squares show AoA_{mean} as a function of *St*, blue diamonds show AoA_{max} as a function of *St* and green triangles show AoA_{mean} as a function of calculated *St* for the downstroke, St_d. Highest angles of attack are at the lowest flight speeds. Values are means; points represent both bats.

stroke plane, may avoid these wake patterns for a larger speed interval than would otherwise be possible. If we compare the values for the calculated St_d and angle of attack with the wake pattern distribution (Fig. 8), all the values except for the lowest speed end up in region C, which is the most efficient region (*St* range 0.2–0.4), with the formation of a stable leading edge vortex (Anderson et al., 1998). Thus, we hypothesize that birds and bats might change their stroke plane with flight speed to maintain a downstroke within a favourable *St* range.

Camber

Camber is a means to increase lift production (Hoerner, 1975). Using our rather rough estimate of camber we found that camber values were higher than those normally found in comparable steady-state wings. However, values of the same magnitude for *G. soricina* flying at 1 m s^{-1} have also been found by Muijres and colleagues (Muijres et al., 2008) using an independent technique. The maximum and mean camber of the wings of the bats decreased linearly with increasing flight speed, which is expected as cambered wings are likely to experience a higher drag and the requirements for a high lift coefficient, C_L, of high cambered wings is reduced with increasing flight speed (Laitone, 1997; Pelletier and Mueller, 2000). At higher speeds the importance of profile drag increases and decreasing the camber will decrease drag. At low speeds higher camber probably allows a higher angle of attack and higher lift coefficients without stalling (Norberg, 1972).

We found that the camber of *G. soricina* varied throughout the wingbeat, which has also been shown for the chocolate wattled bat and little bent-wing bat (*Miniopterus australis*) (see Swartz et al., 2006). The camber at mid-downstroke decreases slightly with increasing flight speed, but the variation was quite low. At the lowest flight speeds the mid-upstroke camber was twice that at mid-downstroke. The mid-upstroke camber decreased radically from low to middle flight speeds (1–4 m s^{-1}) and continued to decline slightly at higher speeds. The initial high values of mid-upstroke camber at low speeds are probably associated with the twist of the wing to allow the handwing to generate lift during the backward flip. The velocities at the armwing are relatively low at this point and a high camber at the armwing decreases the frontal area, lowering drag, as the wing is moved back. The high values of camber may also just be a consequence of twisting the wing along the span. Either way it explains why the camber decreases rapidly with increasing speed, when the back-flick motion disappears.

Wake comparison

For comparison of the wake-width and wingspan we simply divided the wingbeat period into six stroke phases, equal in duration. This is a rough division as the stroke phases are unlikely to be exactly equal and the definition of the periods may vary between kinematics and wake studies. The wake has been described in detail previously (Johansson et al., 2008). As this result is based on data for only one bat, it should be interpreted with caution. However, we found that the width of the wake followed the changes in the wingspan closely, particularly during the downstroke. For the upstroke, there is initially a difference between the wingspan and the wake width, which increases further during the course of the upstroke. At this phase of the wingbeat the tip vortices are relatively close to each other and the lower wake width could be a due to interaction between the tip vortices. However, to determine whether this is the case further studies are necessary, where a higher time resolution of the DPIV (Hedenström et al., 2009; Hubel et al., 2009) will allow for a more detailed correlation between kinematics and wake. At the mid-upstroke, at 4 m s^{-1}, the data correspond well. At the end of upstroke the wingspan is increasing and becoming similar to the values at the beginning of the downstroke, whereas the wake width is decreasing. This last difference is caused by the definition of the wake width, which ignores the negative lift-inducing vortex ring generated at the handwing, and measures the width between the vortices of the same sense of circulation as the tip vortex generated mid-span. Overall, the wake data reflect the actual wing movement quite well.

In steady level flight the total weight *W* has to be balanced by the lift. For steady-state wings operating at similar Reynolds number *Re* the lift coefficient increases with increasing angle of attack, and with increasing camber at a given angle of attack (Laitone, 1997; Pelletier and Mueller, 2000). As a simple way to describe the relationship between the measured wake circulation, body geometry and weight we examined the relationship between the normalized circulation and the mean angle of attack and the camber during mid-downstroke (Fig. 9), using circulation values from the start vortex and the total measured circulation (Γ_{tot}). Both increased camber and angle of attack were associated with increased circulation and thus a higher lift coefficient (Fig. 9). At the theoretical U_{mp} ($U_{mp}\approx 6.8$ m s^{-1} for both bats), the $\Gamma/Uc\approx 0.31$ and thus the time-averaged $C_L\approx 0.62$ (Rosén et al., 2007). This is higher than for a number of bird species, flying at calculated U_{mp}, where the time-averaged lift coefficient is approximately 0.4 (Spedding et al., 2008). Spedding and colleagues showed that the circulation from the start and stop vortices alone is not sufficient for weight support in a bird at slow speeds, and that one has to take into account the vorticity shed at the transition between downstroke and upstroke and into the upstroke (Spedding et al., 2003). This normalized Γ_{tot} yields significantly higher estimates of C_L than estimates based on start vortices alone (Fig. 9). At the theoretical U_{mp}, the estimated $C_L\approx 1.7$ when using normalized Γ_{tot}. At the lowest flight speeds, when both camber and the angle of attack are highest, the estimated values of C_L for our bats were greater than 4 (Γ/Uc) and 10 (Γ_{tot}/Uc), respectively. Fixed wings

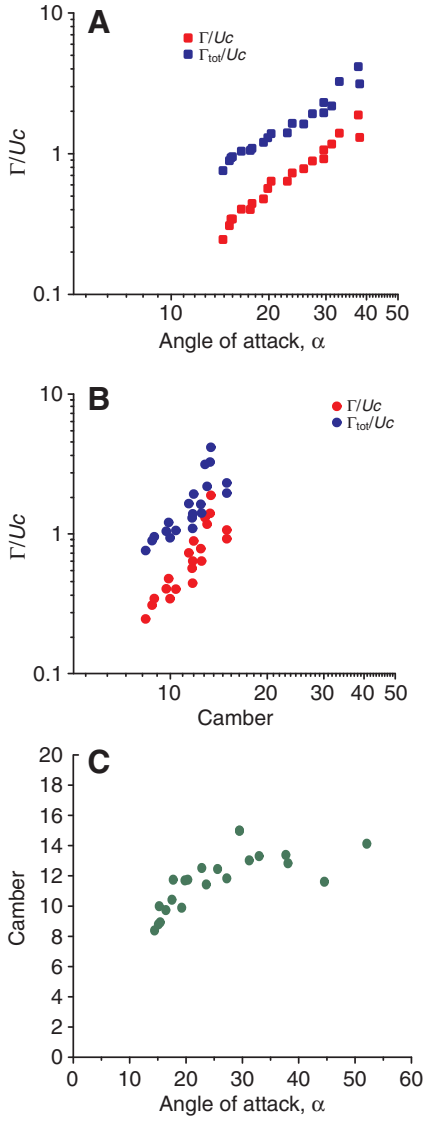

Fig. 9. Normalized circulation from start vortices (Γ/Uc – red) and total measured circulation (Γ_{tot}/Uc – blue) as a function of mean angle of attack (A) and camber at mid-downstroke (B), plotted on a log–log scale. (C) Camber at mid-downstroke as a function of angle of attack. The points represent values for both bats.

of similar aspect ratio and at a similar *Re* have been shown to generate lift coefficients below or up to 1.6 (Laitone, 1997; Pelletier and Mueller, 2000) under steady conditions. The values estimated for the bats are a lot higher, which indicates the presence of high-lift mechanisms at low flight speeds. Although the comparison with steady plates might not be completely ideal, the notion that the mechanics might be unsteady is also supported by the high values of Strouhal numbers at low speeds, the high values of camber and angle of attack and the presence of a leading-edge vortex as shown by Muijres and colleagues (Muijres et al., 2008).

Concluding remarks

Depending on flight speed, flying animals can adjust the lift and power output in many ways by varying different kinematic parameters. In this paper we have shown that the variation of the kinematics of *G. soricina* is continuous and follows the patterns observed by our previous studies of the wake. In particular, the changing function of the upstroke is repeatedly reflected by the different kinematic parameters.

Connecting wake structure and wingbeat kinematic studies gives a more powerful picture of what happens during wingbeats at different flight speeds and makes it easier to draw conclusions and create models that hopefully will increase our understanding of aerodynamic mechanisms of flight. Our results are based on only two individuals of one bat species and should therefore be followed up by studies of more individuals and species. However, they indicate that the flight pattern of birds and bats may differ in several aspects in their kinematics. The wing morphology of the bats influences their flight and thus also kinematic parameters such as the span ratio, which is more similar to that of swifts and hummingbirds, than to passerine birds. The high values of angle of attack, camber and Strouhal number together with the wake geometry all indicate that the flight of these bats is governed by an unsteady high-lift mechanism at low flight speeds. Ideally our detailed record of the kinematics of flight of *G. soricina* will allow for a better comparison with existing bird data and hopefully with other studies of bat flight in the future.

LIST OF SYMBOLS AND ABBREVIATIONS

A_x	horizontal flapping amplitude
A_z	tip-to-tip amplitude
b	half wingspan
$2b$	wingspan
c	mean chord
C_L	lift coefficient
f	wingbeat frequency
L	lift
q	dynamic pressure
r.m.s.	root mean square
Re	Reynolds number
S	wing area
SR	span ratio
SR_{arm}	span ratio for the armwing
SR_{hand}	span ratio for the handwing
St	Strouhal number
St_d	Strouhal number for the downstroke
St_u	Strouhal number for the upstroke
T	stroke period
T_d	downstroke period
T_u	upstroke period
U	forward velocity
U_{mp}	minimum power speed
W	weight
z_{tip}	vertical wingtip position
α	angle of attack
β	stroke plane angle
γ	body tilt angle
Γ	circulation
Γ_{tot}	total measured circulation
θ	wing stroke amplitude
τ	downstroke ratio

ACKNOWLEDGEMENTS

This work was supported by grants from the Swedish Research Council, the Swedish Foundation for International Cooperation in Research and Higher Education, the Knut and Alice Wallenberg Foundation, the Crafoord Foundation, the Magnus Bergvall Foundation, the Royal Physiographic Society in Lund and the Volkswagen Stiftung.

REFERENCES

Aldridge, H. D. J. N. (1986). Kinematics and aerodynamics of the greater horseshoe bat, *Rhinolophus ferrumequinum*, in horizontal flight at various flight speeds. *J. Exp. Biol.* **126**, 479-497.

Aldridge, H. D. J. N. (1987). Body accelerations during the wingbeat in six bat species: the function of the upstroke in thrust generation. *J. Exp. Biol.* **130**, 275-293.

Anderson, J. M., Streitlien, K., Barrett, D. S. and Triantafyllou, M. S. (1998). Oscillating foils of high propulsive efficiency. *J. Fluid. Mech.* **360**, 41-72.
Brown, R. H. J. (1953). The flight of birds. II. Wing function in relation to speed. *J. Exp. Biol.* **30**, 90-103.
Bullen, R. D. and McKenzie, N. L. (2002). Scaling bat wing beat frequency and amplitude. *J. Exp. Biol.* **205**, 2615-2626.
Hedenström, A., Rosén, M. and Spedding, G. R. (2006). Vortex wakes generated by robins *Erithacus rubecula* during free flight in a wind tunnel. *J. Soc. Interface* **3**, 263-276.
Hedenström, A., Johansson, L. C., Wolf, M., von Busse, R., Winter, Y. and Spedding, G. R. (2007). Bat flight generates complex aerodynamic tracks. *Science* **316**, 894-897.
Hedenström, A., Muijres, F., von Busse, R., Johansson, C., Winter, Y. and Spedding, G. R. (2009) High-speed stereo DPIV measurements of bat wakes flying freely in a wind tunnel. *Exp. Fluids* **46**, 923-932.
Hedrick, T. L., Tobalske, B. W. and Biewener, A. A. (2002). Estimates of circulation and gait change based on a three-dimensional kinematic analysis of flight in cockatiels (*Nymphicus hollandicus*) and ringed turtle-doves (*Streptopelia risoria*). *J. Exp. Biol.* **205**, 1389-1409.
Henningsson, P., Spedding, G. R. and Hedenström, A. (2008). Wortex wake and flight kinematics of a swift in cruising flight in a wind tunnel. *J. Exp. Biol.* **211**, 717-730.
Hoerner, S. F. (1975). *Fluid-Dynamic Lift: Practical Information on Aerodynamic and Hydrodynamic Lift*, 2nd edn (ed. H. V. Borst). New Jersey: L. A. Hoerner.
Hubel, T. Y., Hristov, N. I., Swartz, S. M. and Breuer, K. S. (2009). Time-resolved wake structure and kinematics of bat flight. *Exp. Fluids* **46**, 933-943.
Hughes, P. M. and Rayner, J. M. V. (1991). Addition of artificial loads to long-eared bats *Plecotus auritus* – handicapping flight performance. *J. Exp. Biol.* **161**, 285-298.
Hughes, P. and Rayner, J. M. V. (1993). The flight of pipistrelle bats *Pipistrellus pipistrellus* during pregnancy and lactation. *J. Zool.* **230**, 541-555.
Johansson, L. C., Wolf, M., von Busse, R., Winter, Y., Spedding, G. R. and Hedenström, A. (2008). The near and far wake of Pallas' long tongued bat (*Glossophaga soricina*). *J. Exp. Biol.* **211**, 2909-2918.
Laitone, E. V. (1997). Wind tunnel tests of wings at Reynolds numbers below 70 000. *Exp. Fluids* **23**, 405-409.
Lentink, D., Van Heijst, G. F., Muijres, F. T. and Van Leeuwen, J. L. (2010). Vortex interactions with flapping wings can be unpredictable. *Biol. Lett.* **6**, 394-397.
Lindhe-Norberg, U. M. and Winter, Y. (2006). Wing beat kinematics of a nectar-feeding bat, *Glossophaga soricina*, flying at different flight speeds and Strouhal numbers. *J. Exp. Biol.* **209**, 3887-3897.
McCormick, B. W. (1995). *Aerodynamics, Aeronautics and Flight Mechanics*. New York: John Wiley and Sons.
Muijres, F. T., Johansson, L. C., Barfield, R., Wolf, M., Spedding, G. R. and Hedenström, A. (2008). Leading edge vortex improves lift in slow flying-bats. *Science* **319**, 1250-1253.
Norberg, U. M. (1972). Bat wing structures important for aerodynamics and rigidity (Mammalia, Chiroptera). *Z. Morph. Tiere.* **73**, 45-61.
Norberg, U. M. (1976a). Aerodynamics, kinematics, and energetics of horizontal flapping flight in the long-eared bat *Plecotus auritus*. *J. Exp. Biol.* **65**, 179-212.
Norberg, U. M. (1976b). Aerodynamics of hovering flight in the long-eared bat *Plecotus auritus*. *J. Exp. Biol.* **65**, 459-470.
Norberg, U. M., Kunz, T. H., Steffensen Winter, Y. and von Helversen, O. (1993). The cost of hovering and forward flight in a nectar-feeding bat, *Glossophaga soricina*, estimated from aerodynamic theory. *J. Exp. Biol.* **182**, 207-227.
Nudds, R. L., Taylor, G. K. and Thomas, A. L. R. (2004). Tuning of Strouhal number for high propulsive efficiency accurately predicts how wing beat frequency and stroke amplitude relate and scale with size and flight speed in birds. *Proc. R. Soc. Lond. B. Biol. Sci.* **271**, 2071-2076.
Park, K. J., Rosén, M. and Hedenström, A. (2001). Flight kinematics of the barn swallow (*Hirundo rustica*) over a wide range of speeds in a wind tunnel. *J. Exp. Biol.* **204**, 2741-2750.
Pelletier, A. and Mueller, T. J. (2000). Low Reynolds number aerodynamics of low-aspect-ratio, thin/flat/cambered-plate wings. *J. Aircraft.* **37**, 825-832.
Pennycuick, C. J. (1989). *Bird Flight Performance: a Practical Calculation Manual*. Oxford: Oxford University Press.
Pennycuick, C. J., Alerstam, T. and Hedenström, A. (1997). A new low-turbulence wind tunnel for bird flight experiments at Lund University, Sweden. *J. Exp. Biol.* **200**, 1441-1449.
Rosén, M., Spedding, G. R. and Hedenström, A. (2004). The relationship between wingbeat kinematics and vortex wake of thrush nightingale. *J. Exp. Biol.* **207**, 4255-4268.
Rosén, M., Spedding, G. R. and Hedenström, A. (2007). Wake structure and wingbeat kinematics of a house-martin *Delichon urbica*. *J. R. Soc. Interface* **4**, 659-668.
Spedding, G. R., Hedenström, A. H. and Rosén, M. (2003). A family of vortex wakes generated by a thrush nightingale in free flight in a wind tunnel over its entire natural range of flight speeds. *J. Exp. Biol.* **2076**, 2313-2344.
Spedding, G. R., Hedenström, A. H., McArthur, J. and Rosén, M. (2008). The implications of low-speed fixed-wing aerofoil measurements on the analysis and performance of flapping bird wings. *J. Exp. Biol.* **211**, 215-223.
Swartz, S. M., Bishop, K. and Ismael-Aquirre, M.-F. (2006). Dynamic complexity of wing form in bats: implications for flight performance. In *Functional Ecology and Evolution of Bats* (ed. A. Zubaid, G. F. McKracken and T. Kunz). Oxford: Oxford University Press.
Taylor, G. K., Nudds, R. L. and Thomas, A. L. R. (2003). Flying and swimming animals cruise at a Strouhal number tuned for high power efficiency. *Nature* **425**, 707-711.
Tobalske, B. W. and Dial, K. (1996). Flight kinematics of black-billed magpies and pigeons over a wide range of speeds. *J. Exp. Biol.* **199**, 263-280.
Tobalske, B. W., Warrick, D. R., Clark, C. J., Powers, D. R., Hedrick, T. L., Hyder, G. A. and Biewener, A. (2007). Three-dimensional kinematics of hummingbird flight. *J. Exp. Biol.* **210**, 2368-2382.
Vogel, S. (1994). Life in moving fluids. Princeton University Press.
von Helversen, O. (1986). Blütenbesuch bei Blumenfledermäusen: kinematik des schwirrfluges und energiebudget im Freiland. In *Biona-report 5, Fledermausflug-bat Flight* (ed. W. Nachtigall), pp. 107-126. Stuttgart: G. Fischer.
Wang, Z. J. (2000). Votrex shedding and frequency selection in flapping flight. *J. Fluid Mech.* **410**, 323-341.
Winter, Y. (1999). Flight speed and body mass of nectar-feeding bats (Glossophaginae) during foraging. *J. Exp. Biol.* **202**, 1917-1930.